

# EPR Spectroscopic Characterization of a Jahn-Teller Distorted ( $C_{3v} \rightarrow C_s$ ) Four-Coordinate Chromium(V) Oxo Species

Troy A. Stich,<sup>[a]</sup> Derek M. Gagnon,<sup>[a]</sup> Bryce L. Anderson,<sup>[b]</sup> Daniel G. Nocera,<sup>[b]</sup> and R. David Britt<sup>\*[a]</sup>

**Abstract:** Metal-oxo coordination compounds have garnered significant interest over the years. The reactivity of the metal-oxo bond is governed by the geometry, charge, spin state, and identity of the other ligands. In this report, we characterize a distorted  $C_{3v}$ -symmetric  $Cr^V$ -oxo complex that has unique magnetic properties, compared with all other known chromyl species. Continuous wave and pulse electron paramagnetic resonance were used to measure the mo-

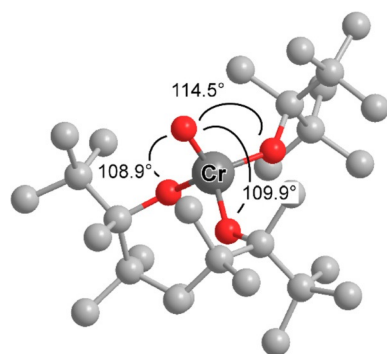
lecular  $g$ -values and  $^{53}Cr$  and  $^{17}O$  hyperfine interactions. Analysis of density functional theory results and the  $g$  and hyperfine tensors, in the context of a crystallographically observed Jahn-Teller distortion, suggests an electronic structure that results from the mixing of two sets of doubly degenerate orbital states. This mixing is only made possible by the approximate three-fold symmetry of the ligand set.

**Keywords:** Chromium · density functional calculations · EPR spectroscopy · Jahn-Teller distortion

## 1 Introduction

Transition metal complexes with terminal oxygen ligands have been, and remain, an exciting medium with which to explore the nuances of ligand field theory.<sup>[1–5]</sup> In particular, the reactivity of the metal-O unit has been shown to be tuned by the nature of the other ligands filling out the coordination sphere, the coordination geometry, and the oxidation state and spin state of the metal ion.<sup>[6–10]</sup> High-valent metal-oxo species are implicated as being involved in many energetically demanding chemical processes, including the oxidation of water. The magnetic properties determined using various spectroscopies, including electron paramagnetic resonance (EPR), have been crucial in deciphering the electronic structures of such metal-oxos and allow predictions to be made concerning their reactivity. We previously prepared the first trigonal  $d^1$   $Cr^V$ -

oxo species (Scheme 1)<sup>[11]</sup> that was shown to have EPR properties unique from all known tetragonal  $Cr^V$ -O complexes, namely a very large  $g$ -shift for  $g_{||}$  and  $g_{||} < g_{\perp}$ . These unusual EPR properties are attributed to the combination of two effects: 1) the presence of only four ligands leads (at least in part) to a reduction in crystal field splitting that allows for the flipping of the  $g$ -tensor anisotropy; and 2) the three-fold symmetry of the ligand set allows two orbital doublets (Scheme 2) to mix, leading to a Jahn-Teller distortion that is observed crystallographically.

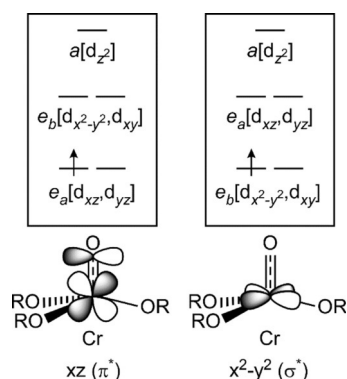


Scheme 1.

[a] T. A. Stich, D. M. Gagnon, R. D. Britt  
Department of Chemistry  
University of California  
One Shields Avenue  
Davis  
CA 95616  
USA  
e-mail: dbritt@ucdavis.edu

[b] B. L. Anderson, D. G. Nocera  
Department of Chemistry and Chemical Biology  
Harvard University  
12 Oxford Street  
Cambridge  
MA 02138  
USA

Supporting information for this article is available on the WWW under <http://dx.doi.org/10.1002/ijch.201600036>.



Scheme 2.

## 2 Methods

### 2.1 Sample Preparation

Solutions of natural abundance  $[\text{Cr}^{\text{V}}(\text{ditox})_3(\text{O})]$  ( $\text{ditox} \equiv \text{Bu}_2(\text{Me})\text{CO}^-$ ) were prepared in toluene, as described previously.<sup>[11]</sup> The  $^{17}\text{O}$ -enriched isotopologue of  $[\text{Cr}^{\text{V}}(\text{ditox})_3(\text{O})]$  was made by reacting  $\text{Cr}^{\text{III}}(\text{ditox})_3$  with  $^{17}\text{O}$ -labeled iodosobenzene (50% enriched) that had been prepared using literature procedures.<sup>[12]</sup> The degree of isotope incorporation was determined by mass spectrometry of the oxidation product of the reaction of  $[\text{Cr}^{\text{V}}(\text{ditox})_3(\text{O})]$  with  $\text{PPh}_3$  (NMR of the starting  $\text{PPh}_3$  reagent indicated that 5% of it was already oxidized to  $\text{OPPh}_3$ ). The isotope pattern for natural abundance  $\text{OPPh}_3$  has two significant peaks: one at 279 m/z with relative intensity 1.0, assigned to the  $\text{H}^+$ -adduct; and one at 280 m/z with relative intensity 0.195, assigned to the  $m+1$   $\text{H}^+$ -adduct. The reaction of  $^{17}\text{O}$ -labeled  $[\text{Cr}^{\text{V}}(\text{ditox})_3(\text{O})]$  with  $\text{PPh}_3$  yielded a mass spectrum for  $\text{OPPh}_3$  with relative intensities of 75.03 and 38.64 for the 279 and 280 m/z peaks, respectively. This intensity pattern corresponds to an  $^{17}\text{O}$ -labeling efficiency of 25.2%. This value was used in simulations of the EPR spectrum of labeled  $[\text{Cr}^{\text{V}}(\text{ditox})_3(\text{O})]$ .

### 2.2 EPR Spectroscopy

The X-band (9.43 GHz) continuous-wave (CW) EPR spectra were recorded on a Bruker (Billerica, MA) Bio-spin EleXsys E500 spectrometer equipped with a super-high Q resonator (ER4122SHQE). Cryogenic temperatures were achieved and controlled using an ESR900 liquid helium cryostat in conjunction with a temperature controller (Oxford Instruments ITC503) and gas flow controller. CW EPR data were collected under slow-passage, non-saturating conditions at a temperature of 80 K. The spectrometer settings were as follows: modulation amplitude = 0.2 mT, and modulation frequency = 100 kHz; conversion time = 88 ms. Pulse  $Q$ -band studies (ca. 34 GHz) were performed using a Bruker E-580 EleXsys spectrometer using a laboratory-built probe<sup>[13]</sup> modified

to fit into an Oxford 935CF cryostat. Temperatures were maintained using an Oxford Instruments ITC503 temperature and gas flow controller. Four-pulse ( $\pi/2$ - $\tau$ - $\pi/2$ - $T$ - $\pi$ - $T$ - $\tau$ - $\pi/2$ - $\tau$ -echo) electron spin-echo envelope modulation (ESEEM) and hyperfine sublevel correlation (HYSCORE,  $\pi/2$ - $\tau$ - $\pi/2$ - $T_1$ - $\pi$ - $T_2$ - $\pi/2$ - $\tau$ -echo) spectroscopies were employed to detect nuclear spin-flip transition frequencies for the hyperfine-coupled  $^{17}\text{O}$  nucleus. Spectral simulations were performed using the Easyspin 5.0 toolbox<sup>[14,15]</sup> within the MatLab software suite (The Mathworks Inc., Natick, MA).

### 2.3 Computational Methods

All calculations were carried out using the ORCA quantum chemistry program.<sup>[16]</sup> The hybrid-functional PBE0 was used in conjunction with unrestricted Kohn-Sham/Hartree-Fock.<sup>[17]</sup> The basis set IGLO-II was used for all carbon and hydrogen atoms, IGLO-III for oxygen atoms, and cc-pCVTZ for chromium.<sup>[18,19]</sup> The conductor-like screening model (COSMO) was used to model the dielectric effects from the solvent toluene.<sup>[20]</sup> The integration grid was expanded around the chromium and oxygen atoms to increase the accuracy of the calculation. EPR properties were calculated using the EPRNMR module in ORCA. The resolution of the identity, chain of spheres approximation (RIJCOSX) was employed.<sup>[21]</sup> A typical input file is included in the supporting information.

## 3 Results and Discussion

The low-temperature CW EPR spectrum of  $[\text{Cr}^{\text{V}}(\text{ditox})_3(\text{O})]$  (Figure 1, top trace) exhibits a slightly rhombic  $g$ -tensor ( $[g_1, g_2, g_3] = [1.9825, 1.9727, 1.9317]$ ). The parallel turning point in the spectrum centered at  $g_3 = 1.9317$  (348.8 mT) is flanked by two clear, low-intensity features at 346.7 mT and 354.3 mT, which would coincide with the second and fourth lines of a hyperfine splitting due to an  $\approx 100$  MHz hyperfine interaction (HFI) with the  $^{53}\text{Cr}$  ( $I = 3/2$ , 9.51% abundant) nucleus. A shoulder appears on the low-field side of the  $g_1$  resonance ( $g = 1.9822$ , 339.9 mT) that suggests  $A_1(^{53}\text{Cr}) \approx 25$  MHz. Alternatively, this shoulder feature could be explained by a 60 MHz  $A(^{53}\text{Cr})$  along  $g_2$ , though this assignment yields an overall less good simulation. The best-fit  $^{53}\text{Cr}$  HFI is found to be  $[A_1, A_2, A_3] = [24(1), 20(10), 103(1)]$  MHz.

The  $[\text{Cr}^{\text{V}}(\text{ditox})_3(\text{O})]$  species is rather unstable<sup>[11]</sup> and decomposes to a variety of species, some paramagnetic (see Figure S2). For example, in the spectrum of  $[\text{Cr}^{\text{V}}(\text{ditox})_3(\text{O})]$  shown in Figure 1, a series of derivative-shaped resonances at 330.1, 332.4, 334.7, and 336.9 mT can be seen. These same features appear much more intensely in the spectrum of another preparation of  $[\text{Cr}^{\text{V}}(\text{ditox})_3(\text{O})]$  that was allowed to sit for an extended period at room-temperature before being frozen (Fig-

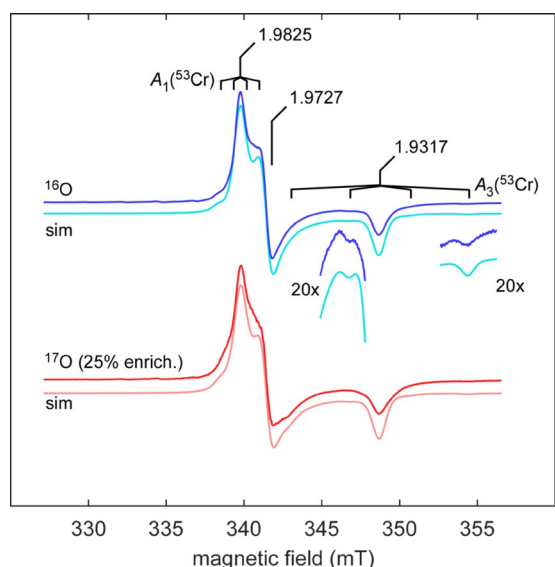


**Figure 1.** CW EPR spectra of  $[\text{Cr}^{\text{V}}(\text{ditox})_3(\text{O})]$  prepared with natural abundance benzyl iodide (top, blue) and with  $^{17}\text{O}$ -enriched benzyl iodide (bottom, red) with the product enriched to a level of 25%. Simulations obtained using parameters given in the text are shown just below each experimental trace. Insets reveal features around  $g_1$  and  $g_3$  that result from  $^{53}\text{Cr}$  hyperfine interaction ( $I=3/2$ , 9.51% natural abundance). Spectrometer settings: microwave frequency = 9.4 GHz; temperature = 80 K; modulation frequency = 100 kHz; modulation amplitude = 0.2 mT; and conversion time = 88 ms.

ure S2, green trace). Other EPR signals also develop after a time (Figure S2, red trace), but neither set of signals overlaps with the  $^{53}\text{Cr}$  hyperfine features discussed above.

The room-temperature EPR spectrum of the  $\text{Cr}^{\text{V}}\text{-O}$  complex (published previously)<sup>[11]</sup> possesses a single derivative-shaped line centered at  $g=1.975$ . This value nearly satisfies the relation  $(g_{\text{iso}})^2 = 1/3 \times ((g_1)^2 + (g_2)^2 + (g_3)^2)$ . This small discrepancy could be a manifestation of how, at room temperature, different conformers on the ground-state adiabatic potential energy surface are thermally accessible (*vide infra*). The room-temperature EPR resonance is flanked by two members of the hyperfine splitting pattern, resulting from an isotropic HFI with the  $^{53}\text{Cr}$  nucleus ( $a_{\text{iso}}(^{53}\text{Cr}) = 46(3)$  MHz). This value for  $a_{\text{iso}}(^{53}\text{Cr})$  arises from Fermi contact (FC) and corresponds to only 0.06 unpaired electrons at the nucleus (using  $a^{\text{FC}} = -748.2$  MHz).<sup>[22]</sup> The total  $^{53}\text{Cr}$  HFI is a combination of isotropic, dipolar, and indirect dipolar contributions. The indirect dipolar contribution is proportional to the magnitude of the corresponding  $g$ -shifts and can be calculated using the anisotropic hyperfine parameter  $P_{\text{d}}(^{53}\text{Cr}) = -103.0$  MHz (specifically,  $P_{\text{d}}[\Delta g_x, \Delta g_y, \Delta g_z]$ ).<sup>[22]</sup> The indirect dipolar contribution is found to be small, relative to the total HFI, whether invoking a  $d_{x^2-y^2}$  ( $A_{\text{ind.dip.}} = [+2, +2, +8]$  MHz) or  $d_{xz}$  ( $A_{\text{ind.dip.}} = [+8, +2, +2]$  MHz) ground-state description. Therefore, solely subtracting off the isotropic element should give a good estimate of the

dipolar part of the  $^{53}\text{Cr}$  HFI, i.e.,  $A_{\text{dip.}} \approx [-25, -25, +50]$  MHz where  $A_{\text{dip.}} \equiv \rho P_{\text{d}} [+2/7, +2/7, -4/7]$  for a ground-state  $[d_{xy}]^1$  electronic configuration, and  $\rho$  corresponds to the population of unpaired spins in the d-orbital that describes that ground state, nearly 1.0 in this case.

Preparation of  $[\text{Cr}^{\text{V}}(\text{ditox})_3(\text{O})]$  using  $^{17}\text{O}$ -labeled iodosobenzene led to incorporation of the magnetic oxygen nucleus ( $I=5/2$ ) at the terminal oxido position (25.2% enrichment). The features of the corresponding CW EPR spectrum (Figure 1, bottom trace) are modestly broadened, compared with the natural abundance isotopologue. The best-fit simulations indicate that  $[A_1, A_2, A_3](^{17}\text{O})$  is roughly  $[13, 13, <10]$  MHz. Due to the incomplete enrichment, it is difficult to determine these parameters more precisely solely on the basis of the CW EPR spectra. However, by performing four-pulse electron spin-echo envelope modulation (ESEEM) in resonance with  $g_3$ , features were apparent only in the spectrum of the labeled compound (*cf.* top and bottom traces in Figure 2). The traces shown in Figure 2 result from the summation of 32 cross-term averaged ESEEM spectra acquired under identical conditions save for the value of  $\tau$ , which was incremented by 8 ns from 200 ns to 456 ns (individual

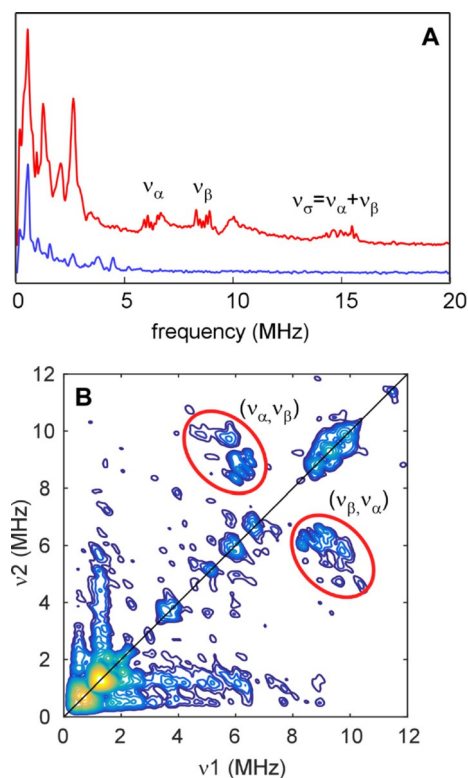


**Figure 2.** A) Sum-over- $\tau$  four-pulse ESEEM spectra of  $^{17}\text{O}$ -labeled (red trace) and natural abundance (blue trace)  $[\text{Cr}^{\text{V}}(\text{ditox})_3(\text{O})]$ . Spectrometer settings: temperature = 25 K; field = 1270 mT; frequency = 34.307 GHz;  $dT = 12$  ns; and  $\tau = 200$  ns incremented by 8 ns up to 456 ns. B) HYSORE spectrum of  $[\text{Cr}^{\text{V}}(\text{ditox})_3(^{17}\text{O})]$ . Spectrometer settings: temperature = 25 K; field = 1270 mT; frequency = 34.307 GHz;  $dT = 12$  ns; and  $\tau = 200$  ns.

ESEEM spectra are presented in Figures S1 and S2). This methodology largely removes any  $\tau$ -dependence of the spectrum and has been shown previously to be adept at revealing the magnetic parameters, and in some cases, the electric quadrupole for hyperfine-coupled  $^{17}\text{O}$  nuclei.<sup>[23]</sup> The red trace in Figure 2 possesses broad peaks centered at 6.3, 8.7, and 10.0 MHz, as well as a broad multiplet centered at  $\approx 15$  MHz, which is assigned to the sum combination band ( $\nu_o = \nu_\alpha + \nu_\beta$ ) of the 6.3 and 8.7 MHz peaks. The hyperfine sublevel correlation (HYSCORE) spectrum acquired at 1270 mT shows that the peaks at 6.3 and 8.7 MHz are correlated and are approximately centered at the  $^{17}\text{O}$  Larmor frequency; thus, these features are assigned to the set of five  $^{17}\text{O}$  NMR transitions within each of the spin-up ( $\nu_\alpha$ ) and spin-down ( $\nu_\beta$ ) electron spin manifolds. Simulation of these correlated peaks requires that the effective  $^{17}\text{O}$  HFI is at  $g_3 \approx 2.5$  MHz. The splitting ( $\Delta\nu_o$ ) between the peaks of the combination band at 15 MHz varies between 0.2 and 0.3 MHz and is related to the magnitude of the nuclear quadrupole interaction (NQI), the shifting of the nuclear spin levels in response to an electric field gradient across the nucleus. Using the relationship  $e^2Qq/h \approx (40/12)\Delta\nu_o$ , the component of the NQI tensor ( $e^2Qq/h$ ) that is probed when in resonance with  $g_3$  is estimated to be  $0.8(\pm 0.2)$  MHz. The  $\nu_o$  peak is not observed in ESEEM/HYSCORE data collected in

resonance with  $g_1$  and  $g_2$ , precluding a more precise estimation of the NQI along these vectors.

The crystal structure of the  $d^1$   $\text{Cr}^{\text{V}}\text{-O}$  complex (Scheme 1) reveals that the pseudo- $C_{3v}$  geometry distorts significantly to  $C_s$  symmetry, as one of the alkoxide  $\text{O}-\text{Cr}-\text{O}$  bond angles increases to  $114.5^\circ$  from an ideal value of  $109.5^\circ$  for a tetrahedral complex (notably, however, a tetrahedral complex would not have the principal axis along the metal-oxo bond), while the isovalent  $d^0$   $\text{V}(\text{V})\text{-O}$  complex maintains  $C_{3v}$  symmetry (avg.  $\text{RO}-\text{V}(\text{V})-\text{O} = 109.6^\circ$ ).<sup>[11]</sup> This symmetry breaking likely results from a Jahn-Teller induced geometric distortion owing to the  $^2\text{E}$  nature of the ground state (Scheme 2 and *vide infra*). DFT geometry-optimization of the  $[\text{Cr}^{\text{V}}(\text{ditox})_3\text{O}]$  structure preserved this distorted geometry (Table S3 in Ref. [11]) and predicted a  $[\text{d}_{xz}]^1$  ground-state description. Population of a  $\text{Cr}-\text{O}$   $\pi^*$   $\text{d}_{xz}$ -based orbital qualitatively explains the long  $\text{Cr}-\text{O}$  bond ( $1.649 \text{ \AA}$ ) and low  $\text{Cr}-\text{O}$  stretching frequency ( $946 \text{ cm}^{-1}$ ).

Several pseudo- $C_4$ -symmetric  $d^1$  systems have been characterized and shown to have a  $[\text{d}_{xy}]^1$  electron configuration in the ground state. Accordingly, these systems exhibit axially symmetric  $g$ -tensors, and when the metal HFI is evident, the largest magnitude element of the hyperfine tensor coincides with  $g_{||}$ , implying that  $g_{||}$  is along the molecular  $z$ -axis (Table 1). Notably, all tetrago-

**Table 1.** Magnetic parameters for Cr(V)-containing and other relevant complexes.

Species	$g$	A (MHz)	$\nu_{\text{M-X}}$ ( $\text{cm}^{-1}$ )	Ref.
$[\text{V}^{\text{V}}\text{OCl}_3]^{2-}$	1.9847, 1.9847, 1.9450	$^{51}\text{V}$ [191, 191, 519]		[36]
$[\text{V}^{\text{V}}\text{O}(\text{H}_2\text{O})_5]^{2+}$	1.9813, 1.9801, 1.9331	$^{51}\text{V}$ [213, 217, 546]		[36]
$[\text{V}^{\text{V}}\text{O}(\text{tpp})]^{[i]}$	1.989, 1.989, 1.964	$^{51}\text{V}$ [162, 162, 477]		[37]
$\text{V}^{\text{V}}\text{O}_2/\text{in SiBEA zeolite}$	1.968, 1.942, 1.803	$^{51}\text{V}$ [890, 918, 753]		[38]
$[\text{Cr}^{\text{V}}(\text{ditox})_3(\text{O})]$	1.9825, 1.9727, 1.9317	$^{53}\text{Cr}$ [24, 20, 103]	946	[11] and this work
PBE0-DFT <sup>[a]</sup>	1.9784, 1.9700, 1.9473	$^{53}\text{Cr}$ [-65, -21, 31]		
PBE0-DFT <sup>[b]</sup>	1.9878, 1.9792, 1.9551	$^{53}\text{Cr}$ [-53, -31, 41]		
$[\text{Cr}^{\text{IV}}(\text{ditox})_3(\text{O})]^-$	$S = 1$		870	[11]
$[\text{Cr}^{\text{V}}\text{OCl}_4]^-$	2.006, 1.979, 1.979	n/d		[39]
$[\text{Cr}^{\text{V}}\text{OCl}_3]^{2-}$	2.008, 1.977, 1.977	$^{53}\text{Cr}$ [108, 30, 30]		[39, 40]
$[\text{Cr}^{\text{V}}\text{OL}]^{-[c]}$	1.987, 1.975, 1.975	$^{53}\text{Cr}$ [108, 21, 21]	994	[41, 42]
$[\text{tBuOCO}]\text{Cr}^{\text{VO}}(\text{THF})$	$g_{\text{iso}} = 1.9770$	$A_{\text{iso}}$ $^{53}\text{Cr} = 53$	988	[43]
$[\text{Cr}^{\text{V}}\text{N}(\text{NCCH}_3)\text{cyclam}]^{[d]}$	1.997, 1.997, 1.965	$^{53}\text{Cr}$ [45, 45, 118]	996	[44]
$[\text{Cr}^{\text{V}}\text{N}(\text{N}_3)\text{cyclam}]^{[e]}$	$g_{\text{iso}} = 1.983$	n/d	967	[44]
$[\text{Cr}^{\text{V}}\text{NCl}_4]^-$	1.993, 1.993, 1.948	$^{53}\text{Cr}$ [62, 62, n/d]		[45]
$[\text{Cr}^{\text{V}}\text{NL}]^{[f]}$	1.992, 1.992, 1.956	$^{53}\text{Cr}$ [62, 62, 123]		[46]
$[\text{Cr}^{\text{V}}\text{N}(\text{oep})]^{[g]}$	1.9945, 1.9945, 1.9583	$^{53}\text{Cr}$ [63, 63, 112]	1017 <sup>[h]</sup>	[47, 48]
$\text{Fe}^{\text{V}}\text{NL}^{[i]}$	2.30, 1.98, 1.98			[30, 49]
$[\text{Fe}^{\text{V}}\text{O}(\text{TAML})]^-$	1.99, 1.97, 1.74	$^{57}\text{Fe}$ [-49, -2, -16]		[50]
$[\text{Fe}^{\text{V}}\text{O}(\text{TMC})(\text{NCCH}_3)]^{2+}$	2.053, 2.010, 1.971	$^{57}\text{Fe}$ [-47, -17, 0]	798	[26]
$[\text{Mo}^{\text{V}}\text{OCl}_3]^{2-}$	1.9632, 1.9400, 1.9400	$^{95}\text{Mo}$ [224, 98, 98]		[36]
$\text{Mo}^{\text{V}}\text{SO}$ high pH	1.9871, 1.9636, 1.9529	$^{95}\text{Mo}$ [163, 75, 34]		[51]
$[\text{Mo}^{\text{V}}\text{O}(\text{SPh})_4]^-$	2.020, 1.982, 1.982	$^{95}\text{Mo}$ [157, 66, 66]		[23]
$\text{Mo}^{\text{V}}\text{XO}$ "very rapid" intermediate	2.025, 1.955, 1.949	$^{95}\text{Mo}$ [133, 55, 57]		[52, 53]
$\text{Mo}^{\text{V}}\text{DMSOR}$ intermediate	1.9988, 1.9885, 1.9722	$^{95}\text{Mo}$ [40, 111, 155]		[54]

[a] DFT performed on model based on crystal structure coordinates. [b] DFT performed on pared-down geometry-optimized model from Ref. [11] (coordinates are listed in Table S3 of Ref. [11]). [c]  $L = \text{trans-bis-(2-ethyl-2-hydroxybutanoato)}$ . [d]  $\text{trans-}[\text{Cr}(\text{N})\text{-(cyclam)}(\text{NCCH}_3)]^{2+}$ . [e]  $\text{trans-}[\text{Cr}(\text{N})\text{-(cyclam)}(\text{N}_3)]^{2+}$ . [f]  $L = \text{N,N'-bis(pyridine-2-carbonyl)-o-phenylenediamido}$ . [g]  $\text{oep} = \text{octylethylporphyrin}$ . [h] value for  $\text{Cr}^{\text{V}}(\text{O})\text{tetraphenylporphyrin}$ . [i]  $L = \text{phenyltris(3-tert-butylimidazol-2-ylidene) borato}$ . [j]  $\text{tpp} = \text{tetraphenylporphyrin}$ .

nal Cr<sup>V</sup>-O complexes studied previously exhibit *g*-anisotropy, in which  $g_{||} > g_{\perp}$ ; for [Cr<sup>V</sup>(ditox)<sub>3</sub>(O)], the opposite is true, signaling a change in the electronic-structure description upon going from tetragonal to trigonal symmetry.

Curiously, this same flipping of the order of  $g_{||}$  and  $g_{\perp}$  is also found when comparing the oxidos with nitridos of a series of tetragonal Cr<sup>V</sup> complexes (*cf.* Table 1). This behavior was attributed to the stronger covalency (via  $\pi$ -bonding) of the Cr–N bond, leading to a large destabilization of the degenerate orbital set  $d_{xz/yz}$ .<sup>[24]</sup> The  $d_{x^2-y^2}$  orbital is at the same time stabilized by deformation of the equatorial plane. According to the ligand field equations used to predict *g*-shifts from  $d \leftrightarrow d$  electronic transition energies (1) and (2) of a  $[d_{xy}]^1$  ion,<sup>[25]</sup>  $g_{||}$  can be less than  $g_{\perp}$  if the  $xy \rightarrow xz/yz$  transition energy is more than one-fourth the energy of the  $xy \rightarrow x^2-y^2$  transition.

$$g_{||} = g_e - \frac{8\lambda\kappa_{\perp}^2}{E_{x^2-y^2} - E_{xy}} \quad (1)$$

$$g_{\perp} = g_e - \frac{2\lambda\kappa_{\perp}^2}{E_{xy/yz} - E_{xy}} \quad (2)$$

Satisfying this condition in the case of [Cr<sup>V</sup>(ditox)<sub>3</sub>(O)] is made easier by the reduction in crystal-field splitting by there being only four ligands. In trigonal symmetry, one expects that the  $d_{xz}$  and  $d_{yz}$  ligand-field excited states will be nearly degenerate (this degeneracy is also expected in the tetragonal complexes), leading to the nearly axial *g*-tensor (2). For trigonal complexes the  $d_{xy}$  and  $d_{x^2-y^2}$  states should also be degenerate (Scheme 2). This latter case of near-degeneracy is responsible for the large  $g_{||}$  shift seen here, consistent with a  $[d_{xy}]^1$  ground-state electron configuration (1).<sup>[1]</sup>

If, however, we consider the possibility of a  $[d_{xz}]^1$  electronic configuration as implied by the DFT results, the ligand field Equations (3) and (4) for calculating  $g_{||}$  and  $g_{\perp}$  are slightly more complicated by the spin-orbit coupling of the  $d_{xz}$  with the  $d_{z^2}$  orbital wavefunctions. In the limit that  $d_{z^2}$  mixing is negligible,  $g_{||}$  can be less than  $g_{\perp}$  when the energy of the  $d_{xz} \rightarrow d_{yz}$  transition is less than the energy of the  $d_{xz} \rightarrow d_{xy/x^2-y^2}$  transition (Eq. 5). In the limit that  $d_{z^2}$  is degenerate with  $d_{xy}$  and  $d_{x^2-y^2}$ ,  $g_{||}$  can be less than  $g_{\perp}$  if the  $d_{xz} \rightarrow d_{yz}$  transition energy is less than one-fourth of the  $d_{xz} \rightarrow d_{z^2/xy/yz}$  transition energy (Eq. 6). Therefore, with nearly degenerate  $d_{xz}$  and  $d_{yz}$  orbitals as noted above, a  $[d_{xz/yz}]^1$  electronic configuration can also result in the observed  $g_{||} < g_{\perp}$ .

$$g_{||} = g_e - \frac{2\lambda\kappa_{||}^2}{E_{xy} - E_{xz}} \quad (3)$$

$$g_{\perp} = g_e - \frac{2\lambda\kappa_{\perp}^2}{E_{xy/x^2-y^2} - E_{xz}} - \frac{6\lambda\kappa_{\perp}^2}{E_{z^2} - E_{xz}} \quad (4)$$

$$g_{\perp} \approx g_e - \frac{2\lambda\kappa_{\perp}^2}{E_{xy/x^2-y^2} - E_{xz}} \rightarrow (E_{z^2} \gg E_{xz}) \quad (5)$$

$$g_{\perp} \approx g_e - \frac{8\lambda\kappa_{\perp}^2}{E_{xy/x^2-y^2/z^2} - E_{xz}} \rightarrow (E_{z^2} \sim E_{xy} = E_{x^2-y^2}) \quad (6)$$

Previous DFT results for [Cr<sup>V</sup>(ditox)<sub>3</sub>(O)] suggested a ground state description of  $[d_{xz/yz}]^1$ , in agreement with the calculations reported in this work.<sup>[11]</sup> If  $g_{||}$  is assigned to  $g_3$ , having the largest part of the <sup>53</sup>Cr HFI along the  $g_z$  axis is inconsistent with a  $3d_{xz}$  ground-state description for the unpaired electron (with  $z$  aligned along the metal-oxo bond), as we would expect  $a_{\text{maximum}}(^{53}\text{Cr})$  to then be along  $g_y$ , perpendicular to the plane of the lobes of the  $d_{xz}$  orbital. Single-point DFT calculations using either the crystal structure coordinates or a fully geometry-optimized model predict that the largest element of a very rhombic <sup>53</sup>Cr hyperfine tensor (Table 1) will be along a vector that bisects two of the Cr–O alkoxide bonds, in the plane of those three atoms, and pointing toward the Cr–O alkoxide with the expanded RO–Cr(V)–O angle (Euler angles for the computed <sup>17</sup>O HFI are  $[-32, 54, -51]^{\circ}$  relative to the *g*-tensor using the  $z$ - $y'$ - $z''$  convention). In other words, the DFT-predicted vector for  $a_{\text{maximum}}(^{53}\text{Cr})$  lies in the plane of the Cr–O  $\pi^*$  MO, not perpendicular to it, and not along the metal-oxo bond vector.

Furthermore, the experimentally-determined <sup>17</sup>O HFI ( $\approx [13, 13, 2.5]$  MHz) is found to be smaller than the computed HFI values and much smaller than if a pure Cr–O  $\pi^*$  molecular orbital was populated with an unpaired electron (*cf.* the strong <sup>17</sup>O HFI in  $[\text{Fe}^{\text{V}}\text{O}(\text{TMC})(\text{NCCH}_3)]^{2+}$ , Table 2).<sup>[26]</sup> The estimate for  $a_{\text{iso}}(^{17}\text{O}) \approx 9.5$  MHz corresponds to merely 0.0018 unpaired electrons at the nucleus<sup>[27]</sup> (using  $a^{\text{FC}} = -5263$  MHz). Subtracting  $a_{\text{iso}}$  from the estimated <sup>17</sup>O hyperfine tensor leaves the hyperfine anisotropy,  $\mathbf{A}_{\text{aniso}} \approx [\pm 3.5, \pm 3.5, \mp 7.0]$  MHz (we do not know the sign of the <sup>17</sup>O hyperfine interaction), is a composed of local ( $\mathbf{T}_{\text{loc}}$ ) and nonlocal contributions ( $\mathbf{T}_{\text{nonloc}}$ ), which are both axially symmetric and traceless tensors that are not necessarily coaxial with one another.<sup>[28]</sup> The nonlocal component ( $\mathbf{T}_{\text{nonloc}} = [+2a, -a, -a]$ ) is simply the through space dipole-dipole interaction between the unpaired electron on the chromium ion and the <sup>17</sup>O nucleus that are separated by  $r = 1.649$  Å, and is computed using the relation  $a = \rho_{\text{Cr}} g_{\text{e}} \beta_{\text{e}} g_{\text{n}} \beta_{\text{n}} / r^3$ . The above analysis of the <sup>53</sup>Cr HFI led to a value for  $\rho_{\text{Cr}} \approx 1.0$ ; therefore, we compute  $a = -2.4$  MHz. Subtracting  $\mathbf{T}_{\text{nonloc}}$  from  $\mathbf{A}_{\text{aniso}}$  gives either  $[-1.1, -1.1, +2.2]$  MHz or  $[+5.9, +5.9, -11.8]$  MHz for  $\mathbf{T}_{\text{loc}}$ , depending on the sign of the measured <sup>17</sup>O HFI.  $\mathbf{T}_{\text{loc}}$  results from spin density in the oxygen-centered *p*-orbitals. Using the tabulated hyperfine value for an electron in an oxygen *2p*-orbital  $P_p = -421.0$  MHz,<sup>[22]</sup> and the angular factors for a *p*-orbital  $(-2/5, -2/5, +4/5)$ , we find

**Table 2.** Magnetic parameters for axial ligand of relevant compounds.

Species	axial ligand	A (MHz)	$e^2Qq/h$ (MHz)	$\eta$	Ref.
[Cr <sup>V</sup> (ditox) <sub>3</sub> (O)]	<sup>17</sup> O	13, 13, 3.5	0.8 (0.2)	n/d	this work
PBE0-DFT <sup>[a]</sup>		0.7, -30.4, 35.5	+3.03	0.39	
PBE0-DFT <sup>[b]</sup>		8.2, 26.4, -32.2	-2.33	0.99	
[Cr <sup>V</sup> N(oep)]	<sup>14</sup> N	10.4, 9.5, 3.6	3.24	0.02	[47]
Fe <sup>V</sup> NL	<sup>14</sup> N	9.11, 6.84, 0.71		n/d	[30]
[Fe <sup>V</sup> O(TMC)(NCCH <sub>3</sub> ) <sub>2</sub> ] <sup>2+</sup>	<sup>17</sup> O	25, 128, 20			[26]
B3LYP-DFT	<sup>17</sup> O	-1.0, -70.8, 75.5			[26]
Mo <sup>V</sup> SO high pH	<sup>17</sup> O	2.4, 1, -3.4	1.6	0.9	[55, 56]
[Mo <sup>V</sup> O(SPh) <sub>4</sub> ] <sup>-</sup>	<sup>17</sup> O	8.1, 4.9, 4.9	1.45	0	[23]

[a] DFT performed on model based on crystal structure coordinates. [b] DFT performed on pared-down geometry-optimized model<sup>[11]</sup> (coordinates are listed in Table S3 of Ref. [11]).

that  $T_{loc}$  corresponds to either 0.007 or 0.035 unpaired electrons in an O 2p orbital, which is very small in either case. So, both the <sup>53</sup>Cr and <sup>17</sup>O HFI appear to be inconsistent with a pure  $d_{xz}$ , Cr–O  $\pi^*$  ground-state description.

Analysis of the spin-down lowest unoccupied MO (LUMO) begins to point to a possible explanation of this incongruity. The LUMO consists of 10% O  $p_{xy}$  character and 40% Cr  $d_{xz,yz}$  character ( $e_a$ , Scheme 2), consistent with the Cr–O  $[\pi^*]^1$  ground-state description. However, DFT also predicts that this LUMO contains 30% Cr  $d_{x^2-y^2,xy}$  character ( $e_b$ , Scheme 2) indicating that there is a propensity for the two doubly-degenerate orbital sets in  $C_{3v}$  symmetry to mix.

This mixing is expected given the geometry of the [Cr<sup>V</sup>(ditox)<sub>3</sub>(O)] complex. McGarvey and Telser provided a quantitative analysis of how “doming” or displacement ( $\Delta$ ) of the central metal ion from the plane formed by the metal-bonding atoms of the three equatorial ligands changes the relative energies of the two doubly degenerate orbital states.<sup>[29]</sup> This analysis was performed for the cases of  $d^4$  and  $d^6$  electron configurations. In [Cr(V)(ditox)<sub>3</sub>(O)], the average value of  $\Delta \approx 21.1^\circ$  is expected to have the  $e_b$  and  $e_a$  orbital sets close in energy to one another, leading to significant unquenched orbital angular momentum in the ground state, and hence, the large  $g$ -shift of  $g_{||}$ . However, a <sup>2</sup>E ground state, by virtue of having one electron (or hole) in two degenerate orbitals is susceptible to Jahn-Teller effects.

A similar result was seen in the DFT-predicted ground state of a  $C_s$  symmetric low-spin  $d^3$  Fe(V)-nitride.<sup>[30]</sup> The mixing of the  $e_a$  and  $e_b$  orbital sets is a Jahn-Teller (JT) effect allowed by the  $C_{3v}$ -parent symmetry of the molecule.<sup>[31]</sup> For this, and other low-spin  $d^3$  trigonal complexes,<sup>[32,33]</sup> it was shown that the combination of the Jahn-Teller distortion and the spin-orbit coupling (SOC) interaction were responsible for the shifting of  $g$ -values away from the free electron value ( $g_e = 2.0023$ ). For the two <sup>2</sup>E configurations depicted in Scheme 2, the JT-SOC effect on the  $g$ -tensor can be parametrized using a fictitious angle  $2\theta$ ,<sup>[32]</sup> where  $\tan(2\theta) \equiv r = \frac{2V}{\lambda}$ .  $r$  represents the ratio between the JT-vibronic induced mixing ( $V$ ) of the

two configurations and the spin-orbit induced angular momentum ( $\lambda$ ). The value for  $\lambda = k\lambda_{free-ion}$ , where  $\lambda_{free-ion} = 380 \text{ cm}^{-1}$  for a Cr(V) ion,<sup>[34]</sup> and  $k$  is the covalency reduction parameter representing loss of chromium character in the electronic-structure description of the ground state due to bonding with ligand atoms. The  $g$ -values can thus be written as functions of  $\theta$  and  $k$ . For the  $[e]^1$  electron configuration exhibited by the Cr(V)-O complex,  $g_{||} = 2(1 - k\cos(2\theta))$  and  $g_{\perp} = 2\sin(2\theta)$ . To match the experimental values of  $g_{||} = 1.9317$  and  $g_{\perp} = 1.9776$ ,  $k = 0.23$  and  $r = 6.625$ . Following the procedures detailed in Ref. [30], the covalency parameter is defined as  $k = (a^2 - \frac{b^2}{2})k_0$ , where  $a^2$  is the contribution of the  $e_a$  orbital set and  $b^2$  is the contribution of the  $e_b$  orbital set to the <sup>2</sup>E ground state (given the condition  $a^2 + b^2 = 1$ ). If  $k_0$  assumes a typical value of 0.9, then the value of  $b^2 \approx 0.5$ , indicating an approximately equal contribution of  $[e_a]^1$  and  $[e_b]^1$  configurations to the ground-state description. This degree of configuration mixing is already reflected, somewhat, in the composition of the singly occupied orbital predicted by single determinant DFT methods, as detailed above. This mixed MO description allows for  $d_{xz/yz}$  orbital character, which is consistent with both the longer Cr–O bond observed by X-ray crystallography and the low Cr–O stretching frequency observed in IR spectroscopy. There has been great success of late in predicting the magnetic properties of electron-configurationally mixed metal complexes using complete active space self-consistent field (CASSCF) calculations.<sup>[30,33,35]</sup> The single determinant DFT results reported here do a fair job of predicting the  $g$ -values of the Cr(V)-O complex (Table 1). However, the predictions of the <sup>53</sup>Cr and <sup>17</sup>O HFI would likely be improved using CASSCF methods.

## 4 Conclusion

Similar to other (pseudo)trigonally symmetric metal complexes with an odd number of electrons in an  $e$ -orbital set, the present Cr(V)-O complex experiences a Jahn-Teller distortion that is evident in the X-ray crystal struc-

ture (Scheme 1). Single-determinant DFT calculations are shown to overestimate the covalency of the Cr–O unit as evidenced by the too-small predicted  $^{53}\text{Cr}$  HFI and too-large predicted  $^{17}\text{O}$  HFI (Tables 1 and 2). Furthermore, the orientation of the experimentally-determined  $^{53}\text{Cr}$  hyperfine tensor is incorrect for a pure  $d_{xz/yz}$ -based orbital description for the ground electronic state. All of the apparent inconsistencies between the DFT-predicted electronic structure description and that implied by EPR results can be resolved if the ground-state description includes more  $d_{x^2-y^2/xy}$  character induced by Jahn-Teller  $e-e$  mixing of the two orbital doublets (Scheme 2). In closing, these pseudo-trigonally symmetric metal-oxo complexes continue to challenge first-order ligand field descriptions<sup>[1]</sup> of their electronic structures. The result of this is that the magnetic properties – metal and oxido hyperfine interactions, in particular – require a multi-determinant explanation.

## Acknowledgements

The spectroscopic work was supported by National Science Foundation under the NSF Center CHE-1305124 (to R.D.B.). The synthetic work was supported by NSF CHE-1464232 (to D.G.N.). The EPR spectroscopy was performed using spectrometers at the CalEPR facility funded by the National Institutes of Health (S10-RR021075) and the NSF (CHE-1048671).

## References

- [1] C. J. Ballhausen, H. B. Gray, *Inorg. Chem.* **1962**, *1*, 111–122.
- [2] T. A. Betley, Q. Wu, T. Van Voorhis, D. G. Nocera, *Inorg. Chem.* **2008**, *47*, 1849–1861.
- [3] S. Shaik, H. Chen, D. Janardanan, *Nat. Chem.* **2011**, *3*, 19–27.
- [4] J. R. Winkler, H. B. Gray, *Struct. Bonding* **2012**, *142*, 17–28.
- [5] K. Ray, F. F. Pfaff, B. Wang, W. Nam, *J. Am. Chem. Soc.* **2014**, *136*, 13942–13958.
- [6] C. V. Sastri, J. Lee, K. Oh, Y. J. Lee, J. Lee, T. A. Jackson, K. Ray, H. Hirao, W. Shin, J. A. Halfen, J. Kim, L. Que Jr., S. Shaik, W. Nam, *Proc. Natl. Acad. Sci. U. S. A* **2007**, *104*, 19181–19186.
- [7] A. S. Borovik, *Chem. Soc. Rev.* **2011**, *40*, 1870–1874.
- [8] D. Janardanan, D. Usharani, S. Shaik, *Angew. Chem. Int. Ed.* **2012**, *51*, 4421–4425.
- [9] S. Fukuzumi, *Coord. Chem. Rev.* **2013**, *257*, 1564–1575.
- [10] D. Mandal, S. Shaik, *J. Am. Chem. Soc.* **2016**, *138*, 2094–2097.
- [11] S. Groysman, D. Villagran, D. G. Nocera, *Inorg. Chem.* **2010**, *49*, 10759–10761.
- [12] B. C. Schardt, C. L. Hill, *Inorg. Chem.* **1983**, *22*, 1563–1565.
- [13] R. Calvo, E. C. Abresch, R. Bittl, G. Feher, W. Hofbauer, R. A. Isaacson, W. Lubitz, M. Y. Okamura, M. L. Paddock, *J. Am. Chem. Soc.* **2000**, *122*, 7327–7341.
- [14] S. Stoll, A. Schweiger, *J. Magn. Reson.* **2006**, *178*, 42–55.
- [15] S. Stoll, R. D. Britt, *Phys. Chem. Chem. Phys.* **2009**, *11*, 6614–6625.
- [16] F. Neese, *Wiley Interdiscip. Rev.: Comput. Mol. Sci.* **2012**, *2*, 73–78.
- [17] C. Adamo, V. Barone, *J. Chem. Phys.* **1999**, *110*, 6158–6170.
- [18] W. Kutzelnigg, U. Fleischer, M. Schindler, *NMR* **1990**, *23*, 165–262.
- [19] R. A. Kendall, T. H. Dunning, R. J. Harrison, *J. Chem. Phys.* **1992**, *96*, 6796–6806.
- [20] A. Klamt, G. Schuurmann, *J. Chem. Soc. Perkin Trans. 2* **1993**, 799–805.
- [21] F. Neese, F. Wennmohs, A. Hansen, U. Becker, *Chem. Phys.* **2009**, *356*, 98–109.
- [22] J. R. Morton, K. F. Preston, *J. Magn. Reson.* **1978**, *30*, 577–582.
- [23] A. V. Astashkin, F. Neese, A. M. Raitsimring, J. J. A. Cooney, E. Bultman, J. H. Enemark, *J. Am. Chem. Soc.* **2005**, *127*, 16713–16722.
- [24] H. Fujii, T. Yoshimura, H. Kamada, *Inorg. Chem.* **1997**, *36*, 1122–1127.
- [25] M. H. L. Pryce, *Proc. Phys. Soc. London Sect. A* **1950**, *63*, 25–29.
- [26] K. M. Van Heuvelen, A. T. Fiedler, X. Shan, R. F. De Hont, K. K. Meier, E. L. Bominaar, E. Muenck, L. Que Jr., *Proc. Natl. Acad. Sci. U.S.A* **2012**, *109*, 11933–11938.
- [27] The induced dipolar coupling of the  $^{17}\text{O}$  HFI is small as it scales with the spin-orbit coupling constant of the nucleus under inspection.
- [28] P. Manikandan, E.-Y. Choi, R. Hille, B. M. Hoffman, *J. Am. Chem. Soc.* **2001**, *123*, 2658–2663.
- [29] B. R. McGarvey, J. Telsler, *Inorg. Chem.* **2012**, *51*, 6000–6010.
- [30] G. E. Cutsail III, B. W. Stein, D. Subedi, J. M. Smith, M. L. Kirk, B. M. Hoffman, *J. Am. Chem. Soc.* **2014**, *136*, 12323–12336.
- [31] I. B. Bersuker, *Jahn-Teller Effect*, Cambridge University Press, Cambridge, **2006**.
- [32] R. L. McNaughton, J. M. Chin, W. W. Weare, R. R. Schrock, B. M. Hoffman, *J. Am. Chem. Soc.* **2007**, *129*, 3480–3481.
- [33] R. L. McNaughton, M. Roemelt, J. M. Chin, R. R. Schrock, F. Neese, B. M. Hoffman, *J. Am. Chem. Soc.* **2010**, *132*, 8645–8656.
- [34] J. Bendix, M. Brorson, C. E. Schaffer, *Inorg. Chem.* **1993**, *32*, 2838–2849.
- [35] F. Neese, T. Petrenko, D. Ganyushin, G. Olbrich, *Coord. Chem. Rev.* **2007**, *251*, 288–327.
- [36] K. DeArmond, B. B. Garrett, H. S. Gutowsky, *J. Chem. Phys.* **1965**, *42*, 1019–1025.
- [37] D. Kivelson, S. K. Lee, *J. Chem. Phys.* **1964**, *41*, 1896–1903.
- [38] P. Pietrzyk, K. Gora-Marek, *Phys. Chem. Chem. Phys.* **2016**, *18*, 9490–9496.
- [39] H. Kon, N. E. Sharpless, *J. Chem. Phys.* **1965**, *42*, 906–909.
- [40] C. R. Hare, H. B. Gray, I. Bernal, *Inorg. Chem.* **1962**, *1*, 831–835.
- [41] M. Krumpolc, B. G. DeBoer, J. Rocek, *J. Am. Chem. Soc.* **1978**, *100*, 145–153.
- [42] M. Branca, A. Dessi, G. Micera, D. Sanna, *Inorg. Chem.* **1993**, *32*, 578–581.
- [43] M. O'Reilly, J. M. Falkowski, V. Ramachandran, M. Pati, K. A. Abboud, N. S. Dalal, T. G. Gray, A. S. Veige, *Inorg. Chem.* **2009**, *48*, 10901–10903.
- [44] K. Meyer, J. Bendix, E. Bill, T. Weyhermuller, K. Wieghardt, *Inorg. Chem.* **1998**, *37*, 5180–5188.
- [45] J. Bendix, *J. Am. Chem. Soc.* **2003**, *125*, 13348–13349.
- [46] N. Azuma, T. Ozawa, S. Tsuboyama, *J. Chem. Soc. Dalton Trans.* **1994**, 2609–2613.

- [47] J. W. Buchler, C. Dreher, K.-L. Lay, A. Raap, K. Gersonde, *Inorg. Chem.* **1983**, *22*, 879–884.
- [48] J. T. Groves, T. Takahashi, W. M. Butler, *Inorg. Chem.* **1983**, *22*, 884–887.
- [49] J. J. Scepaniak, C. S. Vogel, M. M. Khusniyarov, F. W. Heinemann, K. Meyer, J. M. Smith, *Science* **2011**, *331*, 1049–1052.
- [50] F. T. de Oliveira, A. Chanda, D. Banerjee, X. Shan, S. Mondal, L. Que, E. L. Bominaar, E. Münck, T. J. Collins, *Science* **2007**, *315*, 835–838.
- [51] M. M. Cospér, F. Neese, A. V. Astashkin, M. D. Carducci, A. M. Raitsimring, J. H. Enemark, *Inorg. Chem.* **2005**, *44*, 1290–1301.
- [52] R. M. Jones, F. E. Inscore, R. Hille, M. L. Kirk, *Inorg. Chem.* **1999**, *38*, 4963–4970.
- [53] G. N. George, R. C. Bray, *Biochemistry* **1988**, *27*, 3603–3609.
- [54] R. P. Mtei, G. Lyashenko, B. Stein, N. Rubie, R. Hille, M. L. Kirk, *J. Am. Chem. Soc.* **2011**, *133*, 9762–9774.
- [55] A. V. Astashkin, C. J. Feng, A. M. Raitsimring, J. H. Enemark, *J. Am. Chem. Soc.* **2005**, *127*, 502–503.
- [56] A. V. Astashkin, E. L. Klein, D. Ganyushin, K. Johnson-Winters, F. Neese, U. Kappler, J. H. Enemark, *Phys. Chem. Chem. Phys.* **2009**, *11*, 6733–6742.

Received: April 22, 2016

Published online: August 8, 2016